

Electronic Supplementary Information

Surface morphology controls water dissociation on hydrated IrO₂ nanoparticles.

Danilo González, Mariona Sodupe, Luis Rodríguez-Santiago, Xavier Solans-Monfort

Departament de Química, Universitat Autònoma de Barcelona, 08193 Bellaterra, Spain

Table of Contents

A) Comparison between PBE-D2 and PBE-D3	S2
B) Nanoparticle Electronic Structure	S3
C) (IrO ₂) ₃₃ -H ₂ O: Spin Polarized Vs. Closed-Shell Calculations.....	S7
D) Thermal effects on the mol and dis forms relative stabilities.....	S9
E) Projected Density of States (PDOS) of Iridium 5d and Oxygen 2p-orbitals.....	S10
F) (H ₂ O) _M -(IrO ₂) _N Optimized Structures.....	S12
G) AIMD Simulation analysis.....	S16
H) References.....	S18

A) Comparison between PBE-D2 and PBE-D3

Table S1. H₂O adsorption energies (in kJ mol⁻¹) on (IrO₂)₃₃ **G**_{4ax/eq} and **I**_{4eq/eq} sites with PBE-D2 and PBE-D3 levels of theory.

Site	Method	E _{mol/mol}	E _{dis/mol}	E _{mol/dis}	E _{dis/dis}
G _{4ax/eq}	PBE-D2	-160.2	-167.8	-159.0	-165.7
	PBE-D3	-152.7	-161.0	-151.4	-158.8
I _{4eq/eq}	PBE-D2	-163.6	-162.6	-162.2	N.A.
	PBE-D3	-159.1	-157.4	-157.1	N.A.

B) Nanoparticle Electronic Structure

The iridium centers of the bulk present a distorted octahedral coordination characterized by a tetragonal compression with two short axial distances and four long equatorial ones. The computed distances (1.980 and 2.013 Å for axial and equatorial oxygen atoms, respectively) are close to the experimentally reported values. Moreover, since Ir⁴⁺ is a d⁵ cation, IrO₂ could present unpaired electrons in its ground state. However, the non-magnetic state is largely more stable than the ferromagnetic one as already reported earlier,¹ the energy differences being 390.4 kJ mol⁻¹.

Figure S1 show the optimized structures of (IrO₂)₃₃ nanoparticles following different strategies (see below) and Figure S2 the Ir-O, Ir-Ir distance and O-Ir-O angle distribution functions. Optimization of the (IrO₂)₃₃ nanoparticle model inside a vacuum cubic box of 30 Å edge, produces an important surface relaxation (Figure S1a) similar to that described previously for RuO₂ nanoparticles:² i) the Ir-O distances of the undercoordinated surface atoms shortens; ii) the Ir-O distances involving singly coordinated oxygens become even shorter (between 1.711 and 1.741 Å); and iii) the O-Ir-O angles of the centers presenting the singly coordinated oxygens vary as a consequence of the fact that iridium adopts a different coordination with respect to the bulk. However, at variance to what is observed for RuO₂ nanoparticles, (IrO₂)₃₃ geometry optimization also implies an important nanoparticle reconstruction around the tip (I_{4eq/4eq}). The bulk Ir-Ir distance between sites I_{4eq/4eq} and K₃ (3.584 Å) reduces almost 1 Å and this leads to the formation of one Ir-Ir bond (2.614 Å). In parallel to the Ir-Ir bond formation, two Ir-O bonds (one per cation) are cleaved (Figure S1a). This results in an important modification of the coordination environment of these sites. Noteworthy, very little geometry differences are found when comparing the non-magnetic structure

with the magnetic one (Figure 1a and 1b) and, in practice, their radial distributions essentially overlap (Figure S2). The spin polarized solution is more stable than the non-polarized one by $119.0 \text{ kJ mol}^{-1}$, suggesting that nanoparticles of this sizes can be magnetic.

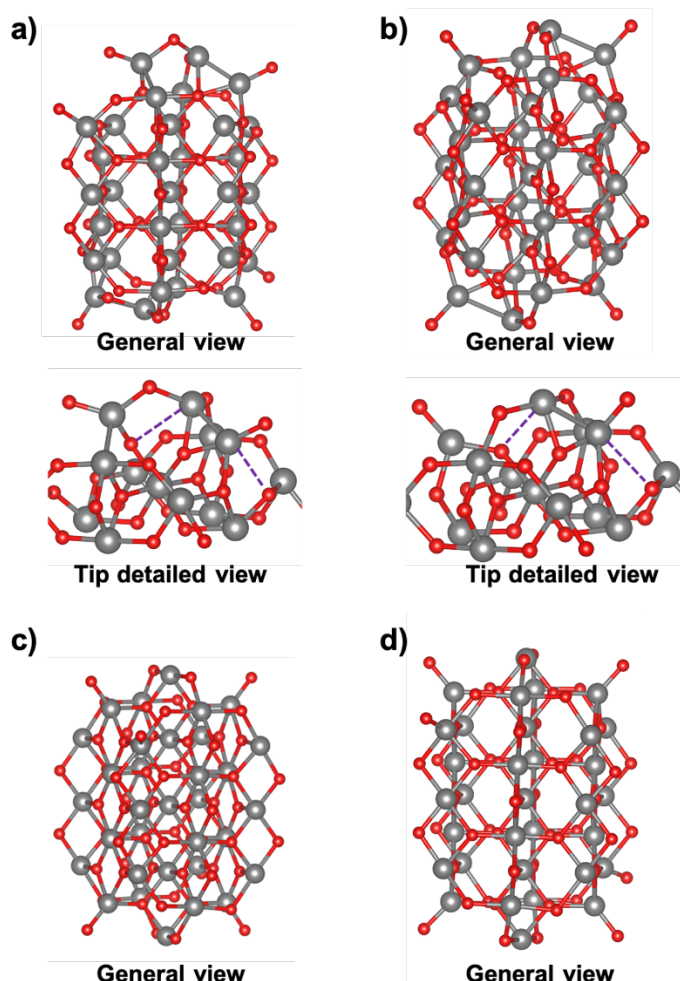


Figure S1. $(\text{IrO}_2)_{33}$ nanoparticle model optimized structure following four different approaches: a) full optimization in vacuum using the spin polarized formalism; b) full optimization in vacuum using the non-spin polarized formalism; c) Constrained optimization with the spin polarized formalism at the $38\text{H}_2\text{O}-(\text{IrO}_2)_{33}$ monolayer structure, where only singly coordinated oxygens are allowed to relax; and d) Constrained optimization with the non-spin polarized formalism at the $38\text{H}_2\text{O}-(\text{IrO}_2)_{33}$ monolayer structure, where only singly coordinated oxygens are allowed to relax. Purple dashed lines indicate Ir-O bonds broken during the geometry optimization.

At this point it is worth mentioning that the synthesis of IrO₂ nanoparticles is usually not performed in vacuum. Indeed, in most cases, the synthesis implies the use of aqueous environments. Thus, the large nanoparticle reconstruction observed when optimizing the (IrO₂)₃₃ nanoparticle model in vacuum may not be realistic. It is for this reason that, we decided to optimize the (IrO₂)₃₃ nanoparticle adding one water molecule per vacant site ((IrO₂)₃₃•38H₂O)). In the initial structure, all water molecules were in its molecular form but some of them spontaneously dissociated during the optimization, this is discussed in the main text. The optimization of the (IrO₂)₃₃•38H₂O model causes major changes on the final structure of the nanoparticle, when compared with the optimization in vacuum (Figure S1c). The addition of solvent molecules is sufficient to prevent the nanoparticle reconstruction. Therefore, the Ir-Ir radial distribution function does not present the small peak at 2.6 Å associated to the Ir-Ir bond formation and one can only observe a small shortening of the Ir-Ir distances (Figure S2). Moreover, the Ir-O distances shortens slightly but Ir-O radial distribution shows a sharper band, in agreement with the absence of Ir-O bond breaking. Finally, the addition of water molecules is sufficient to retain a distorted octahedral coordination geometry on all surface iridium centers, including those presenting singly coordinated oxygen atoms. Overall, the nanoparticle model choice is key for obtaining one or another (IrO₂)₃₃ nanoparticle structure. The optimization including solvent molecules is more realistic since the nanoparticle synthesis is mainly performed in aqueous solution. Unfortunately, the simulation including several water molecules is complex due to the large number of possible conformations (see below) and the higher computational cost. Moreover, it does not allow to analyze the intrinsic Ir-H₂O interaction in each site. Thus, we decided to adopt an intermediate strategy by performing constrained optimizations.

We take as nanoparticle structure that of the optimized $(\text{IrO}_2)_{33} \bullet 38\text{H}_2\text{O}$ model (without the water molecules) and fix all atoms except the singly coordinated oxygens. With the constrained optimizations, the magnetic nanoparticle is more stable than the close shell solution by 25.2 kJ mol^{-1} . The highest spin densities are located at iridium centers located at the tip, those the Ir-Ir implies the coupling of unpaired electrons found in the non-fully relaxed structure.

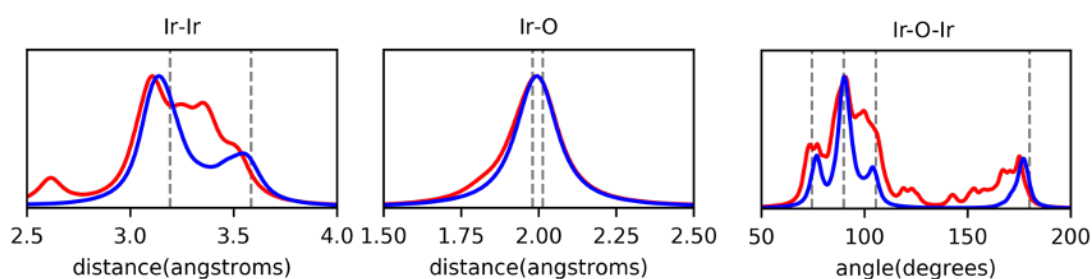


Figure S2. Ir-O, Ir-Ir distance and Ir-O-Ir angle distribution functions for $(\text{IrO}_2)_{33}$ nanoparticle model optimized structure: (red) full optimization in vacuum using the spin polarized formalism; (blue) constrained optimization with the spin polarized formalism at the $38\text{H}_2\text{O}-(\text{IrO}_2)_{33}$ monolayer structure, where only singly coordinated oxygens are allowed to relax. The closed-shell full optimization in vacuum and the close shell optimization of the structure resulting from the nanoparticle – water monolayer system overlap with the red and blue curves, respectively.

C) $(\text{IrO}_2)_{33}\text{-H}_2\text{O}$: Spin Polarized vs. Close-shell Calculations

With the aim of optimize the computational approach for studying larger nanoparticle models and perform ab-initio molecular dynamics for the $(\text{IrO}_2)_{33}\bullet 38\text{H}_2\text{O}$ system, we analyzed the influence of nanoparticle magnetism on the adsorption energy. Table S1 reports the water adsorption energies at the six different sites of $(\text{IrO}_2)_{33}$, the main geometrical features associated to this interaction and the spin density of the iridium centers where the water adsorption occurs. Regardless of the nanoparticle site, the Ir-O distance is similar with the two computational protocols, the largest difference being 0.04 Å. The spin polarized formalism leads to marginally lower adsorption energies, the differences ranging from 0.0 to 12.0 kJ mol⁻¹. The largest energetic differences are observed for site $I_{4\text{eq}/\text{eq}}$, which shows the largest spin densities over iridium. Therefore, it appears that magnetization has a subtle effect on the absolute adsorption energies. In addition, comparison of the relative stabilities between the molecular and dissociated forms at each nanoparticle site shows that the preferred conformation does not change when changing the computational approach. More importantly, the differences between the two structures are essentially not affected (less than 1.4 kJ mol⁻¹). Finally, comparison between the different sites reveal that both the spin-polarized and the non-spin polarized formalism show that the strongest interaction between iridium and undercoordinated iridium centers of the nanoparticle surface occurs when involving iridium atoms at $A_{5\text{ax}}$ and $B_{5\text{ax}}$ sites and the weakest ones when occurring on iridium atoms of site $C_{5\text{eq}}$. Indeed, trends are all conserved, suggesting that close – shell calculations can be used to analyze thermal effects and the influence of nanoparticle size. In this context, all calculations reported in the main text are close-shell.

Table S2. H₂O adsorption energies on (IrO₂)₃₃ sites, main geometrical parameters associated to H₂O adsorption and magnetization over the iridium center adsorbing water obtained with the spin-polarized (close shell) formalisms. All Energies are in kJ mol⁻¹ and the interatomic distances in Å.

Site	Ads. form	E _{ads}	Ir-O _w	H...O	μ ^a
A_{5ax}	dis	-229.8	1.990	1.775	0.0
		(-232.6)	(1.992)	(1.773)	
B_{5ax}	dis	-225.5	1.984	1.800	-0.1
		(-229.2)	(1.986)	(1.794)	
C_{5eq}	mol	-133.6	2.130	2.061	0.1
		(-138.2)	(2.128)	(2.050)	
	dis	-148.7	1.956	2.212	
		(-153.0)	(1.957)	(2.206)	
G_{4ax/eq}	mol	-172.3	2.137	1.732	-0.3
		(-172.3)	(2.128)	(1.724)	
	dis	-187.8	1.983	1.556	
		(-189.2)	(1.946)	(2.367)	
	mol/mol	-158.5	2.142/2.122	1.712/1.606	
		(-160.2)	(2.144/2.115)	(1.711/1.589)	
	mol/dis	-157.0	2.131/2.004	1.691/1.635	
		(-159.0)	(2.133/2.004)	(1.692/1.635)	
dis/mol	-165.7	1.969/2.120	2.165/1.625		
	(-167.8)	(1.968/2.117)	(2.184/1.593)		
dis/dis	-163.5	1.965/2.001	2.052/1.601		
	(-165.7)	(1.965/2.000)	(2.056/1.604)		
I_{4eq/4eq}	mol	-169.0	2.066	1.427	-1.1
		(-181.0)	(2.062)	(1.410)	
	dis	-175.1	1.983	1.556	
		(-187.1)	(1.982)	(1.556)	
	mol/mol	-158.5	2.104/2.089	1.688/1.549	
		(-163.6)	(2.104/2.092)	(1.678/1.559)	
	mol/dis	-157.3	2.131/2.004	1.691/1.635	
		(-162.2)	(2.110/2.009)	(1.716/1.406)	
dis/mol	-157.7	1.969/2.120	2.165/1.625		
	(-162.6)	(2.007/2.098)	(1.443/1.595)		

^a Average value considering all equivalent iridium centers.

D) Thermal effects on the mol and dis forms relative stabilities

Table S2. Thermal effects at 1 atm and different temperatures on the relative energies with respect to the **mol/mol** structure (in kJ mol^{-1}) of the different adsorption forms on **G_{4ax/eq}** and **I_{4eq/eq}** sites of (IrO₂)₃₃ nanoparticle.

Structure	$\Delta(\Delta E)$	$\Delta(\Delta E + \text{ZPE})$	$\Delta(\Delta G^{\circ}_{273})$	$\Delta(\Delta G^{\circ}_{298})$	$\Delta(\Delta G^{\circ}_{323})$	$\Delta(\Delta G^{\circ}_{373})$
G_{4ax/eq}-mol/mol	0.0	0.0	0.0	0.0	0.0	0.0
G_{4ax/eq}-mol/dis	2.4	1.2	1.1	1.3	1.4	1.4
G_{4ax/eq}-dis/mol	-15.1	-15.4	-15.1	-15.8	-15.9	-16.1
G_{4ax/eq}-dis/dis	-11.0	-12.8	-12.7	-12.9	-13.0	-13.1
I_{4eq/eq}-mol/mol	0.0	0.0	0.0	0.0	0.0	0.0
I_{4eq/eq}-mol/dis	3.0	-1.9	-1.8	-2.1	-1.7	-1.6
I_{4eq/eq}-dis/mol	2.0	-2.7	-2.7	-2.6	-2.8	-2.8

E) Projected Density of States (PDOS) of Iridium 5d and Oxygen 2p-orbitals

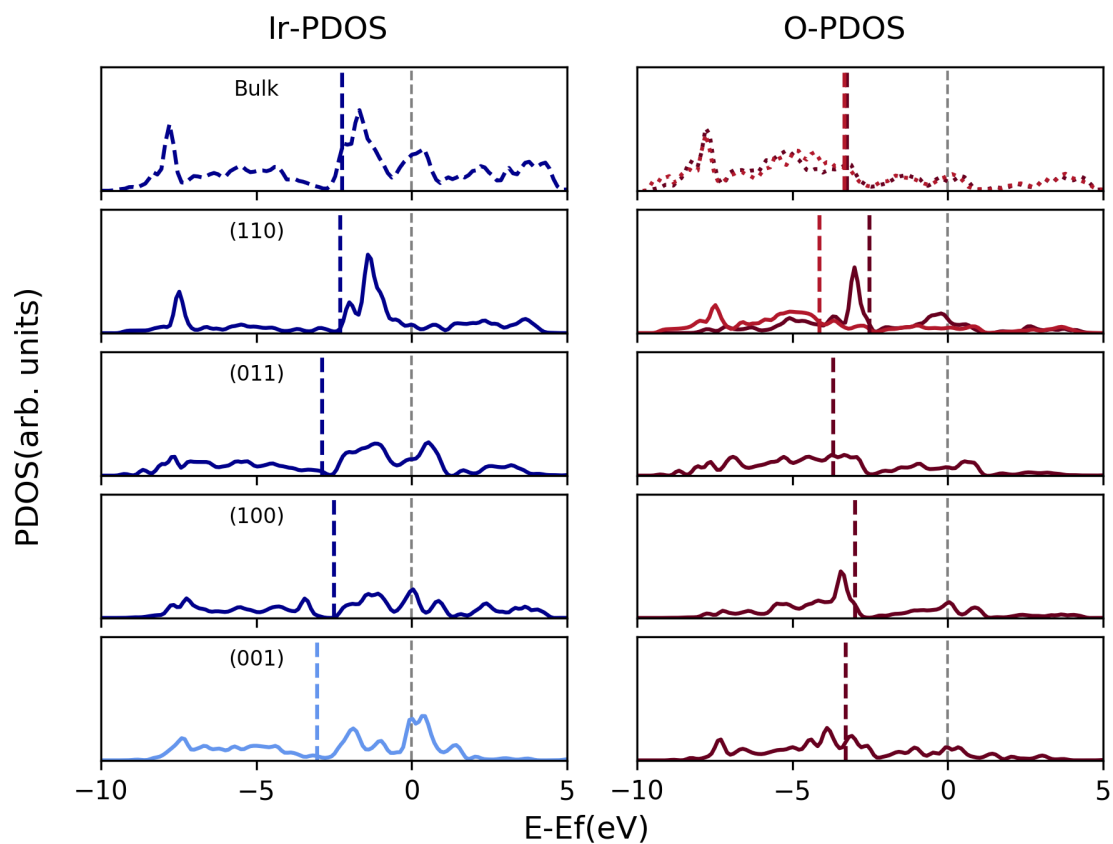


Figure S3. Projected Density of States (PDOS) and the associated band centers of the iridium d- and oxygen p-orbitals of the atoms involved in the H₂O adsorption at the different main crystallographic facets.

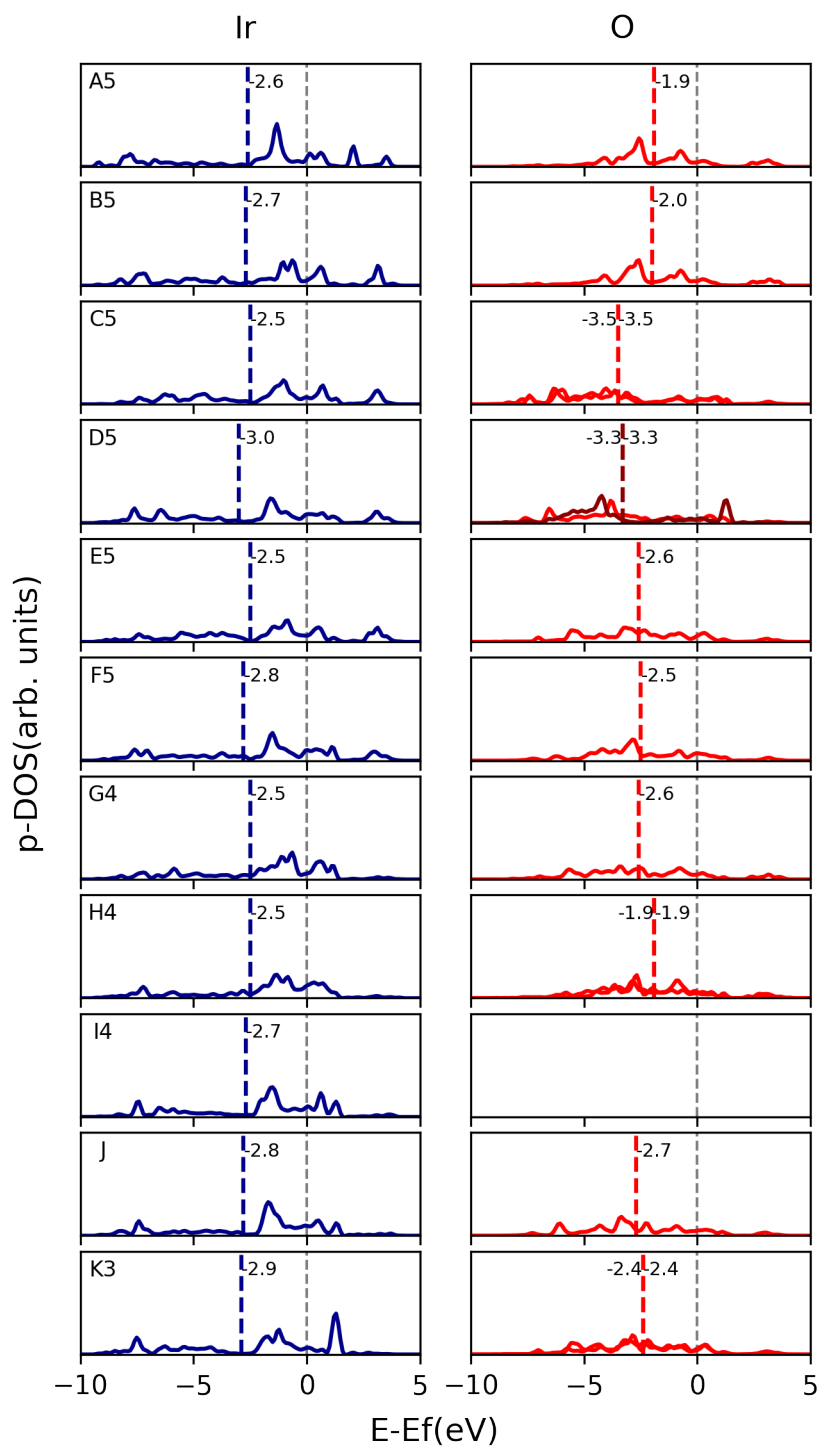


Figure S4. Projected Density of States (PDOS) and the associated band centers of the iridium d- and oxygen p-orbitals of the atoms involved in the H₂O adsorption at the different (IrO₂)₁₁₅ nanoparticle sites.

F) $(\text{H}_2\text{O})_M\text{-(IrO}_2)_N$ Optimized Structures

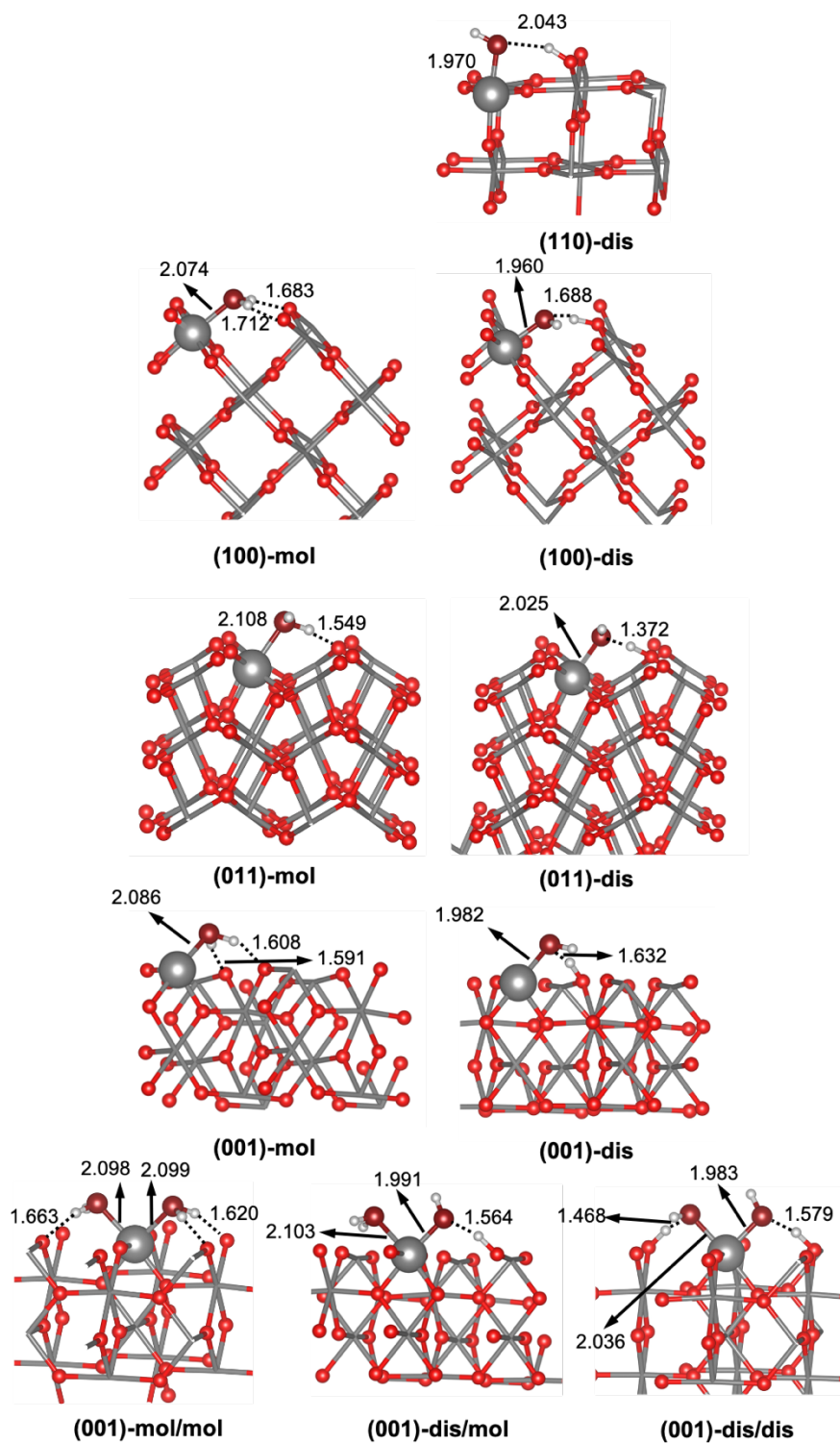


Figure S5. Optimized structure for the molecular and dissociated water adsorption at the different IrO_2 main crystallographic facets. Distances are in Å

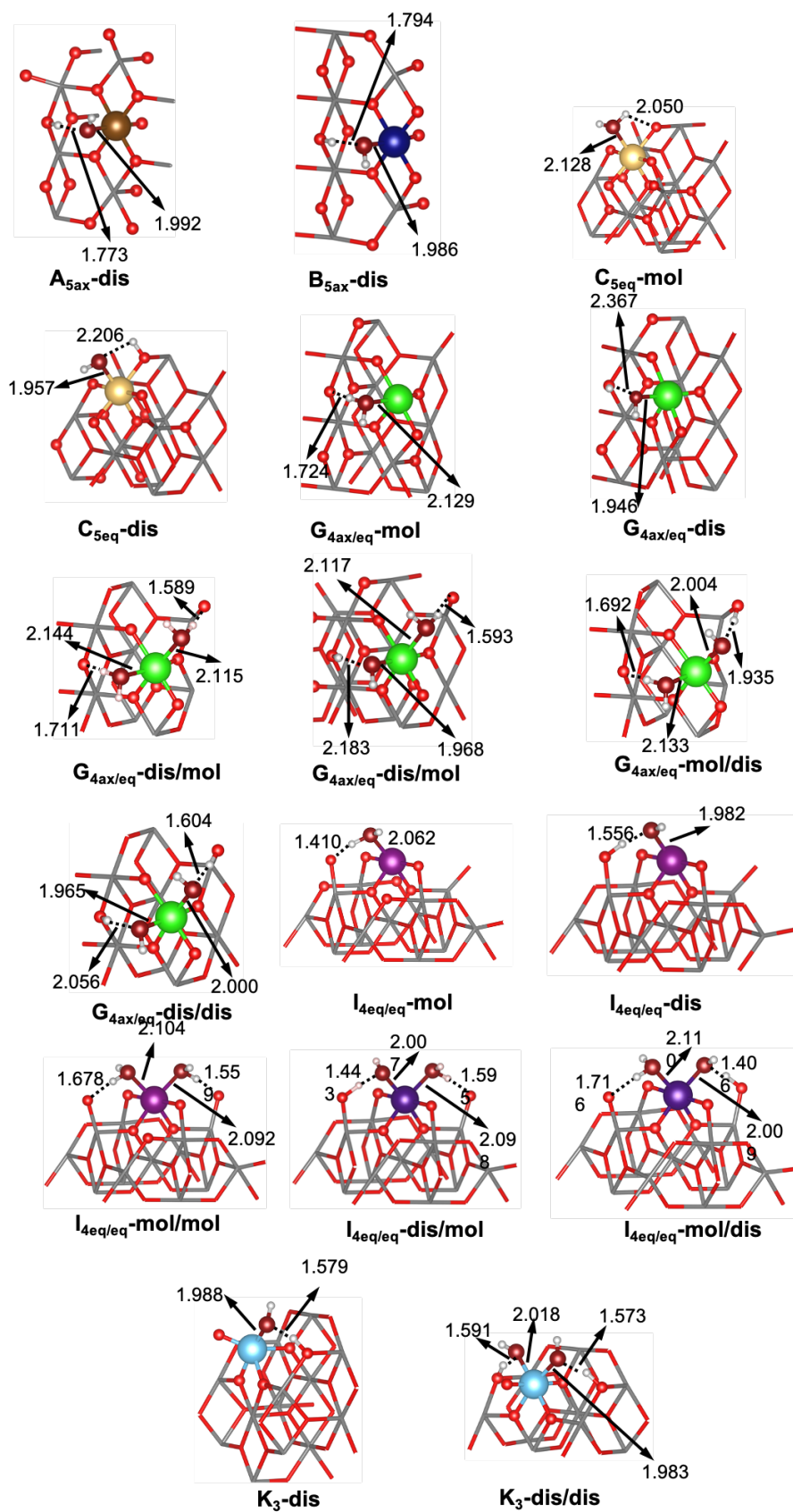


Figure S6. Optimized structure for the molecular and dissociated water adsorption at the different $(\text{IrO}_2)_{33}$ nanoparticle sites. See Figure 1 for labelling. Distances are in Å

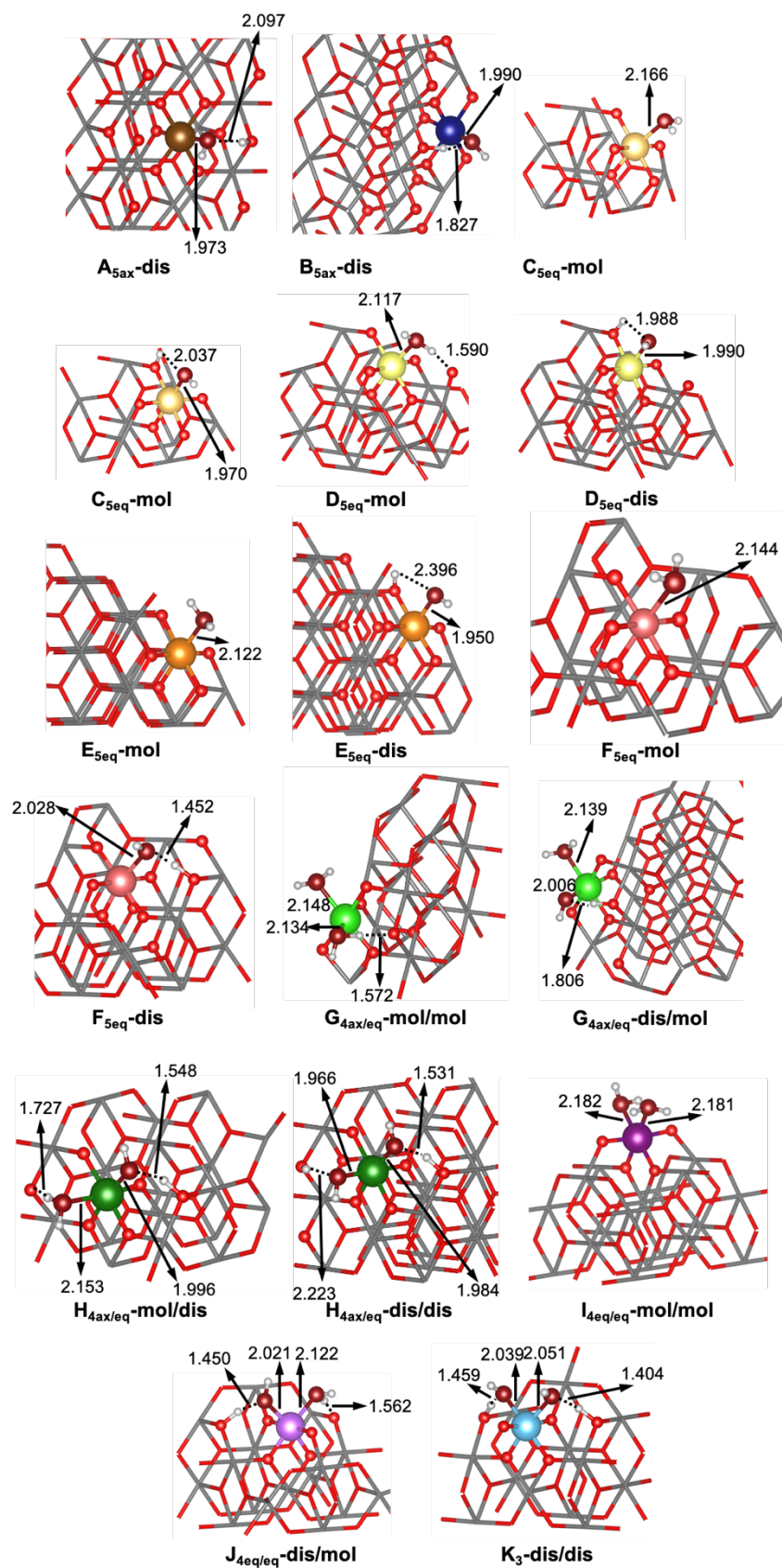


Figure S7. Optimized structure for the molecular and dissociated water adsorption at the different $(\text{IrO}_2)_{115}$ nanoparticle sites. See Figure 1 for labelling. Distances are in \AA

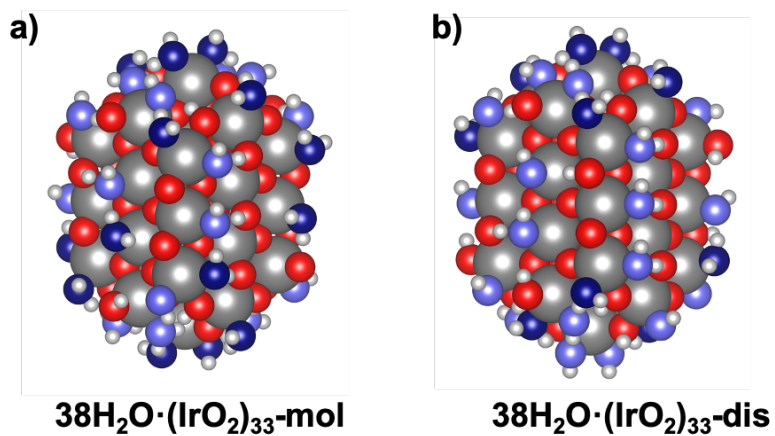


Figure S8. Optimized structure for the 38H₂O·(IrO₂)₃₃ monolayer system starting from two limit initial situations: a) all adsorbed molecules are in their mol form and b) the maximum number of dissociated water molecules are adsorbed to surface iridium centers (28 dis/10 mol). Dark blue atoms correspond to oxygens of adsorbed water molecules, while the light blue atoms correspond to oxygens of the OH- groups.

G) AIMD simulation analysis

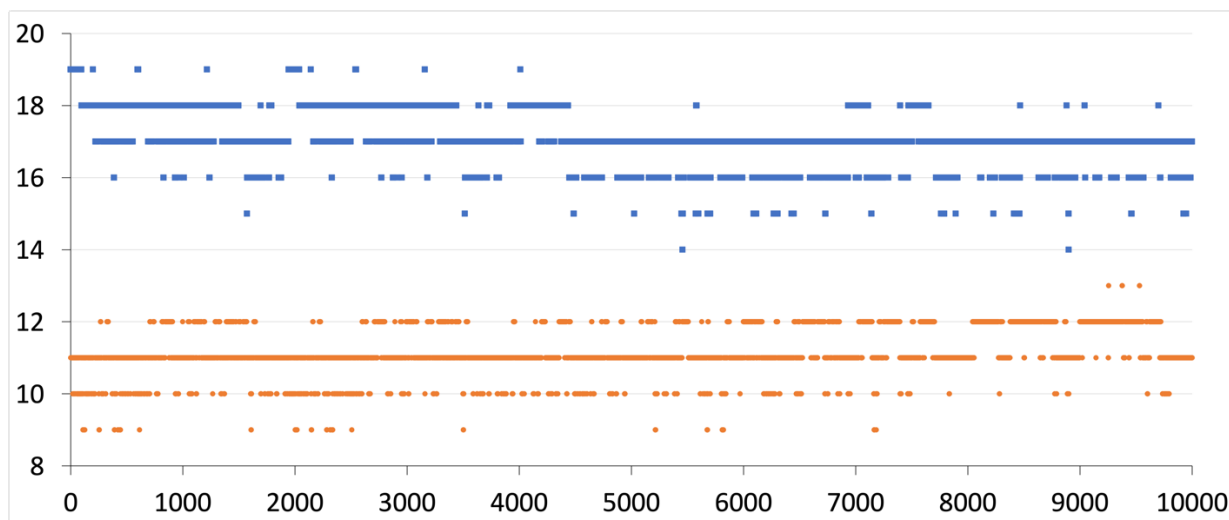


Figure S9. Number of water molecules on the nanoparticle surface along the AIMD simulation. In blue, AIMD simulation starting from a **19mol/19dis** structure; in orange, AIMD simulation starting from a **11mol/27dis** structure.

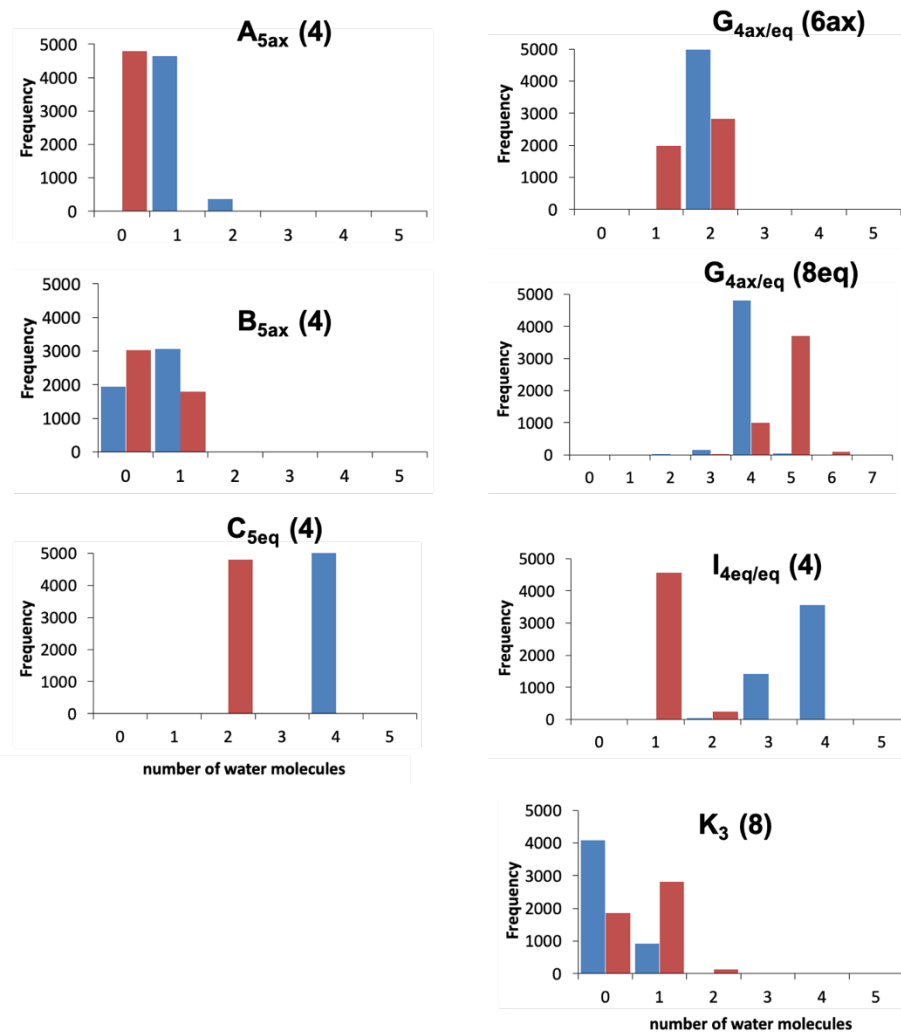


Figure S10. Frequency of the different number of water molecules at each type of site. Bars in blue correspond to the AIMD simulation with a larger fraction of molecular waters, while the bars in red correspond to the simulation starting from a large degree of dissociation.

H) References

- 1 Y. Ping, G. Galli and W. A. Goddard, *J. Phys. Chem. C*, 2015, **119**, 11570–11577.
- 2 D. González, B. Camino, J. Heras-Domingo, A. Rimola, L. Rodríguez-Santiago, X. Solans-Monfort and M. Sodupe, *J. Phys. Chem. C*, 2020, **124**, 1227–1237.